

International Conference on Space Optics—ICSO 2012

Ajaccio, Corse

9–12 October 2012

Edited by Bruno Cugny, Errico Armandillo, and Nikos Karafolas



Wide spectral range imaging interferometer

A. Barducci

D. Guzzi

C. Lastri

V. Nardino

et al.



Wide Spectral Range Imaging Interferometer

A. Barducci, D. Guzzi, C. Lastri, V. Nardino, I. Pippi
Consiglio Nazionale delle Ricerche
Istituto di Fisica Applicata “Nello Carrara”
Sesto Fiorentino, Italy
d.guzzi@ifac.cnr.it

Abstract— In this paper we propose an instrument which is based on a similar payload developed in the framework of the MIOSAT mission of the Italian Space Agency. The instrument is designed on the basis of the following goals: low cost, modularity, plug and play capability, and it should have both wide spectral and spatial range coverage. It will be therefore developed following a modular concept in order to achieve a hyperspectral imager working from visible near infrared up to thermal infrared region.

Index Terms—Fourier transform imaging spectrometers, Sagnac interferometer, Optical design

I. INTRODUCTION

Imaging interferometry is an emerging technique for Earth observation that in the recent past has been demonstrated by dual-use technological space missions [1, 2].

In this paper we propose an instrument which is based on a similar payload developed in the framework of the MIOSAT mission of the Italian Space Agency.

The instrument is designed on the basis of the following goals: low cost, modularity, plug and play capability, and it should have both wide spectral and spatial range coverage.

To this purposes the utilization of an infrared imaging interferometer is expected to be compliant with the previous goals producing the following advantages:

- Gather target spectra at higher spectral resolution as compared with that from dispersive instruments
- Improve the retrieval accuracy of the temperature as well as the emissivity spectrum;
- Enhance the sensor capability to map atmospheric absorption features.

The wide spectral range imaging interferometer will be therefore developed following a modular concept in order to achieve a hyperspectral imager working from visible near infrared up to thermal infrared region.

The instrument concept is based on the common-path Sagnac configuration. It will acquire target images modulated by a pattern of autocorrelation functions of the energy coming from each scene pixel. The resulting fringe pattern remains spatially fixed with respect to the instrument’s field-of-view.

The complete interferogram of each target location is retrieved by introducing a relative motion between the target and the observer, which allows any image pixels to be observed under different viewing-angles and experience discrete Optical Path Differences (OPD). The optical configuration avoids the entrance slit, allowing a higher signal to noise ratio with respect to other imaging spectrometer configurations.

The modular imaging interferometer will be based on two Sagnac blocks one for the visible near infrared part, realized using refractive optics, and one for the medium and thermal infrared range, built using mirrors.

In order to associate the related spectrum (in wavenumber units) to each pixel of the scene, the following data processing steps are performed: starting from dark signal subtraction; instrument spatial response compensation; interpolation and re-assembling of the data cube; DC offset subtraction; apodization; and finally Inverse Fourier Transform. At this point, the radiometric correction procedure is performed. After correcting the at-sensor radiance data from atmospheric effects and ground reflection contributions, the temperature and emissivity of the target can be estimated by applying a data processing algorithm which introduces some a-priori information. The related remote sensing products (temperature and emissivity spectrum) are useful for applications related to climate, volcanoes, HTEs, and so forth. Investigation of atmospheric composition would require instead the use of the at-sensor radiance only, a type of data that does not imply the temperature / emissivity separation step.

II. INSTRUMENT CONCEPT

An image interferometer in the common path Sagnac configuration acquires target images modulated by a pattern of autocorrelation functions of the electromagnetic (EM) power entering the instrument FOV. The complete interferogram of any target locations can be reconstructed introducing source-observer motion, which allows each pixel to be observed while crossing the entire interference fringe pattern. The Sagnac imaging interferometer optical layout working in the leap frog configuration is shown in Fig. 1.

Light is collected from the objective L, then the two interfering rays are generated by the beam-splitter BS and travel the triangular ray path in opposite directions by means of two folding mirrors M1 and M2. The two rays are then focused onto the CCD by the camera lens P. It is easy to demonstrate that the BS is the fundamental component, which provides the basic phase-delay between the two coherent rays. Nonetheless, it can be shown that phase-delay is heavily affected by the overall instrument geometry: the BS to M1 and M2 distances and the orientation of the two folding mirrors. As long as a narrow FOV is imaged the instrument produces a stationary pattern of interference fringes of almost equal thickness (Fizeau fringes) on its output port. The performed implementation of our Sagnac layout doesn’t include any input slit. The Optical Path Difference (OPD) between the

recombining beams linearly changes with the angle (slope) of the entering ray onto the instrument optical axis. It can be shown that the BS provides part of the phase-delay between the two interfering rays, the remaining part being originated outside the BS, and that the overall OPD linearly changes with varying the angle of the entering ray with respect to the instrumental optical axis [3-5]. Due to the absence of entrance slit the device acquires the image of the target superimposed to a fixed pattern of interference fringes.

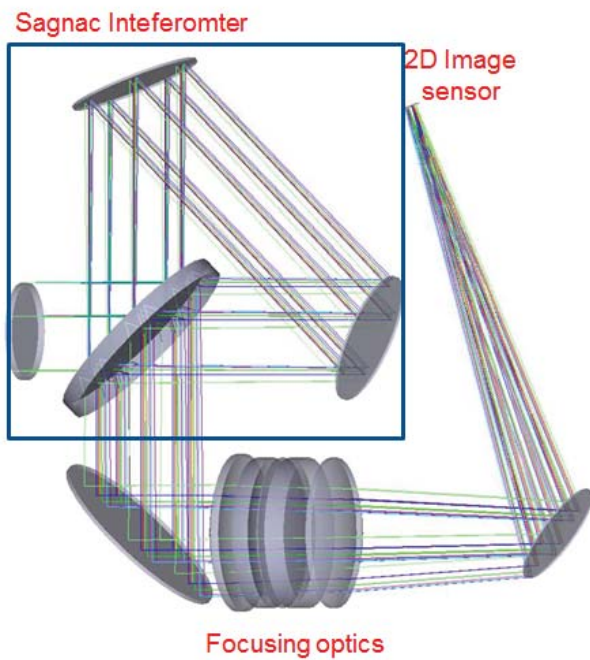


Figure 1. Optical layout of the prototype of a stationary interferometer in Sagnac triangular configuration. Collimated light selected from the input pupil is subject to amplitude separation by the beam-splitter. The two resulting beams (reflected and transmitted) travel the instrument on the same triangular path limited by the folding mirrors. The camera lenses focus the target image onto the detector.

Introducing a relative motion between the sensor and the object, each scene pixel crosses the entire interference pattern; hence its interferogram can be retrieved from an image sequence gathered at the apt frame rate. In a different wording, every target point is observed under several viewing angles while the sensor moves, and three-dimensional array of data (image stack) of varying OPD is collected. This data volume can then be processed in order to interpolate the full interferogram of each image pixel.

The airborne prototype operating in the visible – near infrared range and developed in the framework of the MIOSAT, has been calibrated and tested during several laboratory measurements [5]. Fig. 2 shows one of the laboratory set-up employed for testing the airborne prototype performances: nine calibrated ceramic tiles have been placed on a motorized sledge and observed under a field of view equal to 11°.



Figure 2. (a): Laboratory set up employed for testing imaging interferometer performances showing both ceramic tiles mounted on the sledge and the interferometer prototype (b): Colored ceramic tiles mounted on the motorized sledge (b).

An example of image sequence acquired during the experiment is shown in Fig. 3. Nine frames of a short sequence of measurements portraying ceramic tiles that were observed for assessing the instrument spectral calibration are plotted. The scene details move from left to right while the pattern of interference fringes remains fixed in the instrument’s FOV, a circumstance that shows the specific characteristics of this type of imaging interferometers.

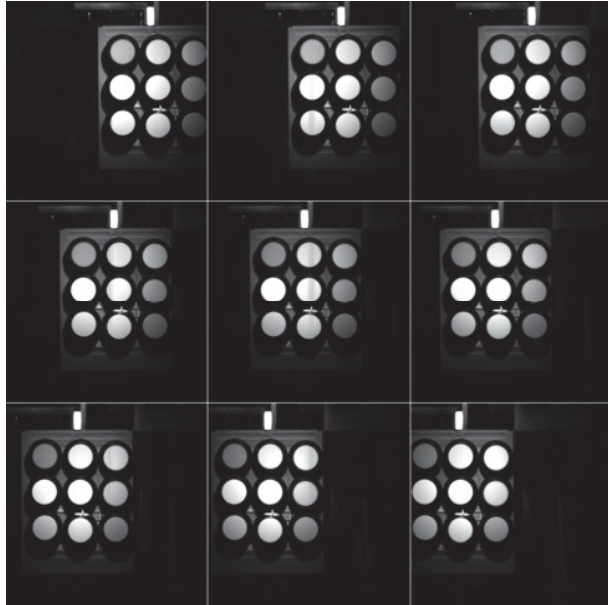


Figure 3. Nine frames of a sequence of measurements portraying ceramic tiles.

Target places observed near the beginning or the end of acquisition usually don’t experience the full range of the OPD, for this reason their interferogram cannot be reconstructed completely, and their spectrum cannot be assessed.

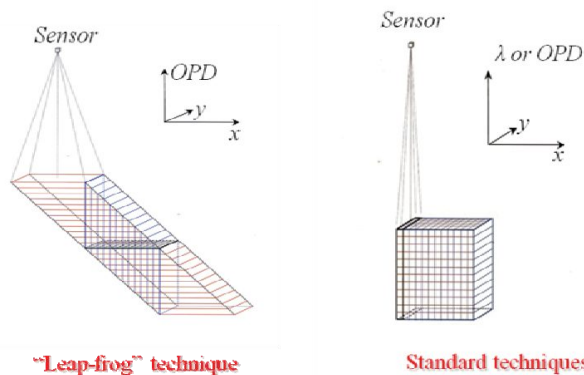


Figure 4. Main differences in data acquisition among Leap-frog and alternative layouts and optical configurations.

The operating feature of the Leap-frog configuration is depicted in Fig. 4, where the main differences in data acquisition among standard and alternative operations are reported. The scheme in the right of the picture represents data acquisition by dispersive pushbroom imaging spectrometers as

well as the acquisition by imaging interferometers equipped with input slit (e.g. FTHSI). As can be seen in the left scheme, the two red sub-volumes at the beginning and at the termination of data acquisition contain pixels that have not travelled the entire range of digitized OPD. The interferogram of these pixels cannot be reconstructed completely, so only partial spectral estimations can be obtained for the conjugated target places.

A. Retrieval of spectral radiance and spectral reflectance

The operating mode of a leap-frog acquisition needs the acquisition of a complete set of frames (data-cube) to reconstruct the full interferogram of the concerned source.

The first step of the processing chain is the alignment of the acquired images related to the observed scene. In this way a data cube containing both the image and the interference of each pixel of the scene is obtained and spatially averaged interferograms can be computed.

The pre-processed interferogram should have a null-mean, starting and ending tails approaching to zero, and any optical artefact removed (e.g. vignetting). In order to achieve this result, we have adopted a pre-processing procedure composed by the following steps [6,7]:

- Dark signal subtraction (i.e.: removing the signal offset in absence of illumination);
- Flat-field calibration
- Instrument spatial response compensation to remove saturated pixels, hot and cold pixels, and pattern noise;
- Radiometric distortion correction to remove effects of vignetting;
- DC offset estimation to remove from the interferogram the band-averaged energy reaching the detector,
- Apodization to mitigate the “Gibbs effect” (ringing phenomenon);
- Optimal spectral estimation.

After subtracting the dark signal image (i.e.: the instrument response in absence of illumination) the gathered images are compensated for possible spatially coherent noise patterns, hot and cold pixels and so forth (flat-field calibration). The reference measurement for the flat-field compensation has been acquired after illuminating with a 500 W halogen lamp the detector through a double diffuser (that simulates an isotropic and spatially uniform extended source).

The procedure described above has been applied to the short sequence of measurements portraying colored calibrated ceramic tiles shown in Fig. 3. As a result, in Fig.5 a frame extracted from the re-assembled image set is shown. It is worth noting that in the re-assembled acquired data-cube, the fringe pattern disappeared showing the goodness of the align procedure.

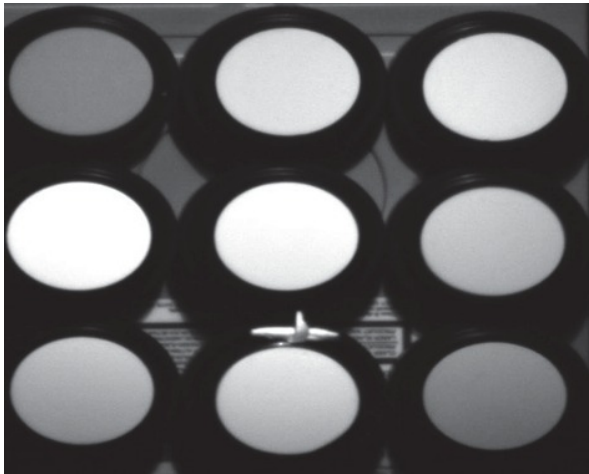
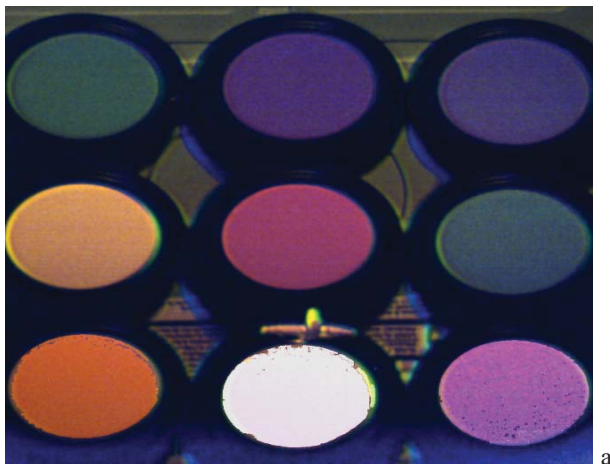
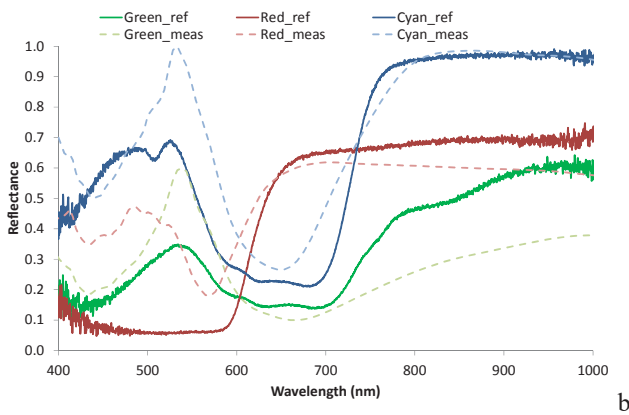


Figure 5 Single frame extracted from the re-assembled data cube where no fringe pattern can be observed..

Spectral reflectance image has been obtained normalizing at sensor radiance using the response coming from the spectralon tile placed in the central lower part of the image in Fig. 5.



a



b

Figure 6(a) RGB of the spectral reflectance hypercube (b) reflectance spectra extracted from ceramic tiles compared with reference measurements.

In Fig.6a the RGB of the reflectance hypercube is reported together with some reflectance spectra extracted from ceramic

tiles (Fig.6b). Spectral reflectance measurements obtained using an Ocean Optics spectrometer USB4000-FL are reported for comparison. It can be noticed the good agreement of the spectral behavior, in particular the red edge starting position for the red tiles spectra, and the position of the peak at 533 nm for both measured and reference value for the green tile spectra.

III. OPTICAL LAYOUTS

As it was shown in the previous chapter, in opposition to dispersive imaging spectrometers, in which the impinging radiance is spectrally dispersed on output focal plane, an imaging interferometer observes the autocorrelation function of the impinging radiation. The acquired physical information is the interferogram $I(x)$, that is the power of the interference pattern generated by the two rays at the position x in the focal plane of the instrument. After retrieving the complete interferogram, the radiance spectrum is reconstructed by applying a Fourier-like inverse transform.

The maximum OPD of the system is linked to the minimum detectable wavelength, being related to the geometry and the dimensions of the internal optical components of the instrument. The spectral range and resolution of the reconstructed spectrum strongly depend on the frame rate (i.e. the number of samples used for interferogram reconstruction) and the range of optical path differences, which in their turn are functions of the instrument field of view, beam splitter features (refractive index, thickness) and detector sampling.

For these reasons a careful design of the optical system, which take into account both optical materials and beam-splitter dimensions, allows the use of the same Sagnac layout both for the realization of an instrument working in the visible-near infrared (VNIR: between 400 nm – 1000 nm), like the realized prototype, or in the medium and thermal infrared range (MIR between 3000 nm and 5000 nm, TIR between 8000 nm and 13000 nm) of the spectrum. TIR interferometry can easily achieve the high spectral resolution needed to estimate the target spectral emissivity and temperature, as well as it is able to overcome the problems related to detector saturation which sometimes affects TIR imaging spectrometry.

TIR spectrometry, both dispersive and Fourier Transform based, is a tool suitable for soil characterization and hazard monitoring [8]. The observation of volcanic activity is another application, in particular infrared remote sensed data can be used to estimate heat flux and thermal features of active volcanoes [9]. Waste areas, study of High Temperature Events (HTE), analysis of thermal anomalies and “heat islands” as well as the temperature distribution in polar regions are other application fields. It is worth noting that accurate land temperature maps covering polar regions are relevant to climate change investigations. Another interesting application of TIR remote sensing is the study of the marine habitat by the measurement of Sea Surface Temperature (SST). TIR spectrometry may also be employed for measuring the total amount of atmospheric gases such as SO_x and NO_x .

Regarding to Felgett’s advantage for imaging interferometer, an analytical comparison of system performance (estimation of amplitude of the effective signal and Signal-to-Noise ratio) between the interferometric

technique and the traditional dispersive spectrometers performed in a previous paper [10], brought to a new interpretation of it, concluding that in the past Fellgett's advantage has been not well understood. In fact the informative tail of the acquired interferogram to be resolved requires a radiometric resolution much finer (depending on the illumination source's bandwidth) than that is needed for a dispersive spectrometer operating at the same high spectral resolution [11]. This fact is particular evident in the visible-near infrared, while a better system performance is expected for those Sagnac imaging interferometers working in the medium – thermal infrared.

In Figure 7 two different optical layouts are shown, one is a lens based configuration designed for a system working in the VNIR range (Fig. 7a), while the other plotted in Fig. 7b is a mirror based configuration developed for an instrument working in the medium and thermal infrared.

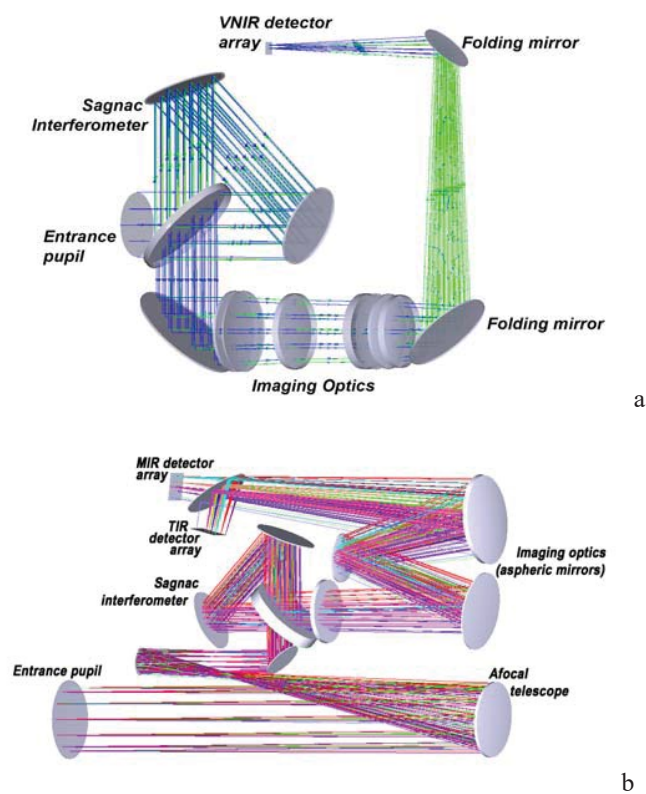


Figure 7. Lens based (a) and mirror based (b) optical system for the imaging interferometer

Some advantages are implicit in using imaging interferometers, due to their high signal (Jacquinot's effect), and the option to adjust the sampled spectral range and resolution by changing the sensor sampling step and the instrument Field-Of-View (FOV). Other critical points are also connected with the high data-rate requested, and the heavy data pre-processing for compensating instrument response and possible acquisition phase errors.

A. Performace simulation in the thermal infrared

In order to investigate the performance of a Sagnac imaging interferometer in the thermal infrared, a ray-tracing simulation software has been developed. This simulation code computes the whole path travelled by any rays entering the interferometer, and accounts for the resulting OPD between the transmitted and reflected rays. Calculation takes into account the dispersion of the material refraction index, as well as the geometrical configuration of the triangular Sagnac (relative positions and orientations of M1, M2 and BS in Figure 1). Relying on the computed OPD, the simulation software calculates the interferogram of a target-source that can be selected by the user among four different models: Gaussian, Black-body, constant, and rectangular sources. Interferogram simulation may include the effect of additive independent Gaussian/uniform radiometric noise. The software also computes the extension required to the optical surfaces in order to mitigate vignetting, and a likelihood estimate of the source spectrum (interferogram inverse cosine transform).

Fig. 8 shows an example of interferogram observed by the instrument equipped with a Germanium BS when imaging a 2-degree wide FOV in the TIR spectral region.

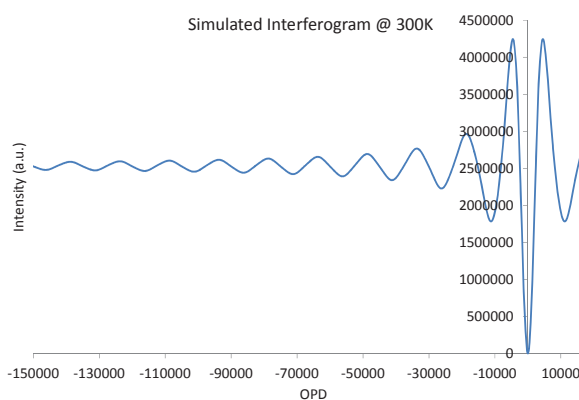


Figure 8 Simulated interferogram for T-ALISEO instrumental configuration with 2° FOV and blackbody source at temperature T = 300°K

The selected source was a black-body at standard the environment temperature T = 300 K. Fig. 9a shows the simulated estimation of the source spectrum in comparison with the actual one. The same type of calculation has been repeated for two black-body sources of higher temperatures and reported in Fig. 9. They can reliably represent the application of a Sagnac imaging interferometer to High Temperature Events (HTE) monitoring. In particular such kind of instrument allows the retrieval of a complete spectrum of the at sensor radiance even if some pixels are saturated.

Let us note that, as usual, the estimated source spectrum is slightly affected by residual ringing.

Simulations as far performed have revealed the feasibility of this kind of interferometric hyperspectral imager, and the advantage of using FT spectrometry in the TIR.

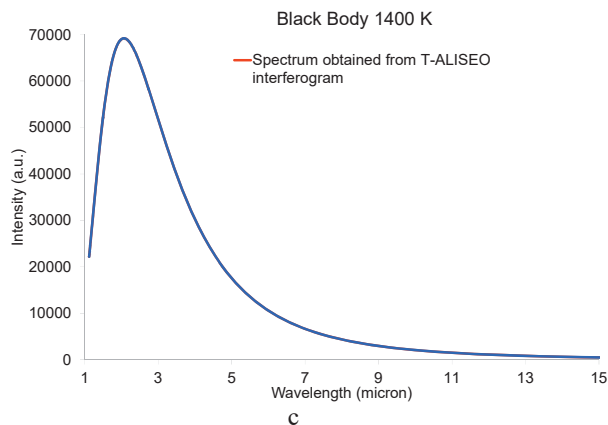
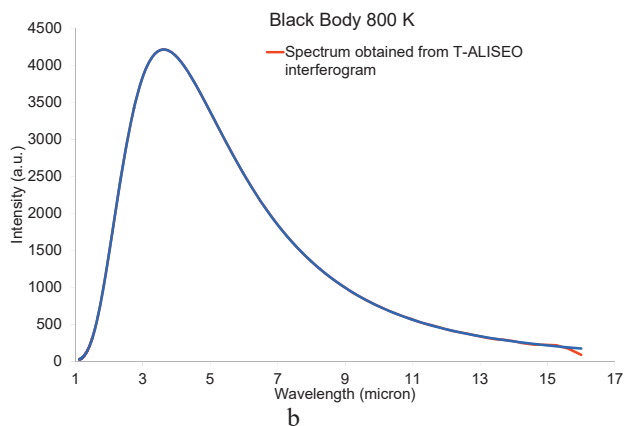
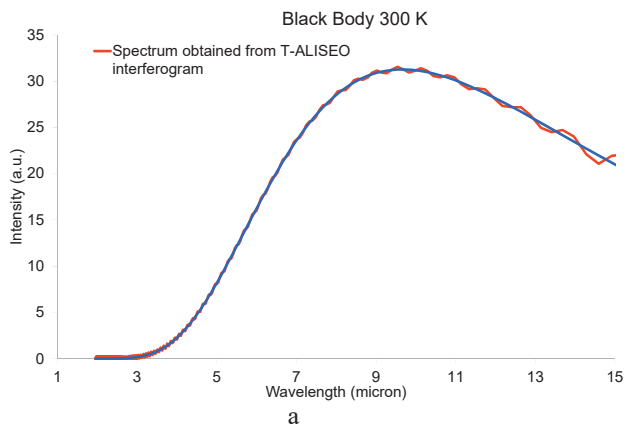


Figure 9. Simulated estimation of the source spectrum in comparison with the actual one blackbody source temperature $T = 300$ °K (a), 800 °K (b), and 1400 °K (c).

IV. DISCUSSION

Some advantages are implicit in using imaging interferometers, due to their high signal (Jacquinot's effect), and the option to adjust the sampled spectral range and resolution by changing the sensor sampling step and the instrument Field-Of-View (FOV). Other critical points are

instead connected with the high data-rate requested, and the heavy data pre-processing for compensating instrument response and possible acquisition phase errors.

Regarding to Felgett's advantage for imaging interferometer, an analytical comparison of system performance (estimation of amplitude of the effective signal and Signal-to-Noise ratio) between the interferometric technique and the traditional dispersive spectrometers performed in a previous paper [5], brought to a new interpretation of it., showing that the informative tail of the acquired interferogram to be resolved requires a radiometric resolution much finer (depending on the illumination source's bandwidth) than that is needed for a dispersive spectrometer operating at the same high spectral resolution [5].

V. CONCLUSIONS

In this paper laboratory measurements performed with a Sagnac imaging interferometer realized in the visible-near infrared have been shown. The analysis of the obtained results confirms the goodness of the processing chain developed for the elaboration of an image acquired by an imaging interferometer in a leap-frog configuration.

The feasibility of a Sagnac imaging interferometer in the thermal infrared has been proved by simulations. In particular simulations show the ability of such kind of instrument to be employed for the detection of high temperature events.

REFERENCES

- [1] M. J. Persky, "A review of spaceborne infrared Fourier transform spectrometers for remote sensing", *Review of Scientific Instruments*, Vol. 66, pp. 4763 – 4797, 1995.
- [2] W. B. Harnisch, E. Hartman, W. Holota, M. Melf, W. Posselt, M. Rost, M. Steiner, H. O. Tittel, W. Weihs, "Compact Fourier Transform Imaging Spectrometer", ESA-CN 14540/00/NL/WK, Proposal No. A.1999-0366-0-1, 1.2.2000 – 31.3.2002, 2002.
- [3] M.-L. Junttila, J. Kauppinen, E. Ikonen, "Performance limits of stationary Fourier spectrometers", *Journal of Optical Society of America A*, vol. 8(9), pp. 1457 – 1462, 1991.
- [4] M. Herring, T. G. Chrien, V. G. Duval, T. N. Kabrach, "Imaging spectrometry: concepts and system trade-offs", in *Infrared and Millimeter-Wave Engineering*, Proc. SPIE 1874, pp. 11 – 23, 1993.
- [5] A. Barducci, D. Guzzi, C. Lastri, P. Marcoionni, V. Nardino, I. Pippi: "Theoretical Aspects of Fourier Transform Spectrometry and Common Path Triangular Interferometers", *Optics Express*, vol. 18(11), pp. 11622 -11649, 2010
- [6] A. Barducci, I. Pippi, "Analysis and rejection of systematic disturbances in hyperspectral remotely sensed images of the Earth", *Applied Optics*, vol. 40, PP. 1464 – 1477, 2001.
- [7] A. Barducci, F. Castagnoli, P. Marcoionni, I.Pippi, "The ALISEO instrument: further improvements of calibration methods and assessment of interferometer response", In "Sensors, Systems, and Next-Generation Satellites XI" edited by R.Meynart, S.P.Neeck, and H.Shimoda, SPIE vol. 5978, pp. 1K – 1-10. Proceedings of SPIE Europe International Symposium on "Remote Sensing", Bruges (B), 19-22 September 2005.
- [8] D.M Tralli.; R.G. Blom, V. Zlotnicki; A. Donnellan; D.L. Evans "Satellite remote sensing of earthquake, volcano, flood, landslide and coastal inundation hazards", *ISPRS Journal Photogramm. Remote Sens.* Vol. 59(4), pp. 185-198, 2005.
- [9] V. Lombardo; M.F. Buongiorno;" Lava flow thermal analysis using three infrared bands of remote-sensing imagery: A case study from Mount Etna 2001 eruption", *Remote Sens. Environ.*, Vol. 101, pp. 141 – 149, 2006.

[10] R. G. Sellar and G. D. Boreman, "Limiting aspect ratio of Sagnac interferometers", *Optical Engineering*, Vol. 42, pp.3320 – 3325, 2003.

[11] A. Barducci, D. Guzzi, C. Lastrì, P. Marcoianni, V. Nardino, I. Pippi: "Radiometric and SNR properties of multiplex dispersive spectrometry", *Applied Optics*, Vol. 49(28), pp. 5366 – 5373, 2010.